PHYSICAL REVIEW E **67**, 045601(R) (2003)

Three-dimensional local density of states in a finite two-dimensional photonic crystal composed of cylinders

D. P. Fussell,[1,*] R. C. McPhedran,[1] C. Martijn de Sterke,[1] and A. A. Asatryan[2]
[1]*School of Physics, University of Sydney, Sydney 2006, New South Wales, Australia*
[2]*School of Mathematical Sciences, University of Technology, Sydney 2007, New South Wales, Australia*
(Received 22 November 2002; published 11 April 2003)

The three-dimensional local density of states (LDOS), which determines the radiation dynamics of a point source, is presented here for a finite two-dimensional photonic crystal as a function of space and frequency. The LDOS is obtained from the dyadic Green's function, which is calculated exactly using the multipole method. Maximum suppression in the LDOS occurs at the high frequency edge of the complete two-dimensional band gap and varies smoothly about this frequency. Macroporous silicon is shown to suppress the LDOS by one order of magnitude at the center of its air pores.

DOI: 10.1103/PhysRevE.67.045601 PACS number(s): 42.70.Qs, 32.80.−t, 42.50.Dv

In the seminal papers by Yablonovitch [1] and John [2], it was proposed that photonic crystals (PCs) can inhibit spontaneous emission and localize light by suppressing the photonic density of states (DOS). Subsequent work using simple models for the DOS has predicted other interesting quantum optical phenomena, including an anomalous Lamb shift [3,4]. In the usual Markovian approximation, the spontaneous emission decay rate is proportional to the DOS. A sufficiently sharp change in the DOS can lead to non-Markovian effects [5], though there is some contention as to whether the models adopted are realistic [6]. Despite the prospect of controlling spontaneous emission, theory and experiment on PCs has been largely confined to band structure calculations, and reflection and transmission spectra (e.g., Ref. [7]). Experiments on spontaneous emission have been conducted using luminescent dye impregnated in colloidal crystals [8] and opals [9], but the interpretation of the results has been impeded by a lack of applicable theory [9]. Furthermore, these experiments probe the DOS, which characterizes spontaneous emission averaged over a unit cell. PCs redistribute the DOS both in frequency and space, and the spatially resolved, or local density of states (LDOS) [10,11], is the fundamental quantity that determines quantum optical behavior.

Probing the LDOS requires measuring the fluorescence from a pointlike source (e.g., luminescent molecule) at some location inside a finite-sized PC. The LDOS can be calculated in infinite PCs using the Bloch method [6,11,12]. Spontaneous emission rates in finite-sized PCs can be obtained using the finite-difference time-domain method [13]. However, this method works in the time domain, and inferring the fundamental LDOS from the emission rates must be justified. The preferred approach is via Green's function. Green's function can be obtained in complex structures by solving Dyson's equation [14], but calculating the LDOS in PCs using this method has been limited to finite one-dimensional structures [15]. It was recently demonstrated that a multipole method can be used to calculate Green's function efficiently in an arbitrary arrangement of aligned circular cylinders of infinite length [16]. This was used to calculate the two-dimensional (2D) LDOS, which applies to an infinite line source, for a finite cluster of cylinders. Thus, all LDOS results published to date are for idealized systems.

Crucial to reconciling experiment with theory is the calculation of the 3D LDOS, which applies to a pointlike source, in realistic PCs. The 3D LDOS is presented here for a 2D PC composed of a finite cluster of circular cylinders of infinite length. The treatment of a dyadic problem in the 3D case constitutes a major extension of the scalar problem in the 2D case, requiring an integration over all propagation constants of the fields using a suitable complex contour. Though 2D PCs do not have the favored complete band gap of 3D PCs, they hold substantial theoretical [17] and experimental [18,19] interest due to the relative ease of their fabrication. The particular 2D PC modeled here is macroporous silicon [19]. This 2D PC is composed of a triangular array of cylindrical air pores in a silicon background, with a pore separation of 1.5 μm and an aspect ratio (pore height to diameter) of 100−500. Reflection and transmission spectra show that this PC is fabricated with a robust 2D band gap. This makes it an essentially ideal 2D PC, to which the results obtained here are directly applicable.

The LDOS $\rho(\mathbf{r},k)$ is determined for a dipole point source from the electric Green's function, $\mathbf{G}^E$, using [20]

$$\rho(\mathbf{r},k) = -\frac{2k}{\pi c^2}\mathrm{Im}\{\mathrm{Tr}[\mathbf{G}^E(\mathbf{r},\mathbf{r};k)]\}, \tag{1}$$

where $k=2\pi/\lambda$ is the free space wave number. In a full vectorial treatment of the fields, Green's functions are in dyadic form [21], and the wave equations for electromagnetic (EM) Green's functions are

$$\nabla\times\nabla\times\mathbf{G}^E(\mathbf{r},\mathbf{r}') - k^2 n(\mathbf{r})^2\,\mathbf{G}^E(\mathbf{r},\mathbf{r}') = -\mathbf{I}\,\delta(\mathbf{r}-\mathbf{r}'), \tag{2}$$

$$\nabla\times\nabla\times\mathbf{G}^H(\mathbf{r},\mathbf{r}') - k^2 n\,(\mathbf{r})^2\mathbf{G}^H(\mathbf{r},\mathbf{r}') = -\nabla\times\mathbf{I}\,\delta(\mathbf{r}-\mathbf{r}'),$$

where $n(\mathbf{r})=n_b$ is the background refractive index and $n(\mathbf{r})=n_l$ inside the cylinders.

*Email address: fussell@physics.usyd.edu.au

Equation (2) is solved in cylindrical coordinates (ρ,ϕ,z), with the cylinder axes aligned with the z coordinate. A Fourier transformation in the z coordinate is first applied, giving wave equations for conical propagation. These are evaluated exactly using the multipole method [22]. A brief summary is given for a source in the background medium, and follows similarly for a source inside a cylinder. For a source in the principal direction $\tilde{\mathbf{u}}$, the z components of the fields are given by

$$(\boldsymbol{\nabla}_{\boldsymbol{\rho}}^2+k_\rho^2)V_u=D_u^V\delta(\boldsymbol{\rho}-\boldsymbol{\rho}'), \tag{3}$$

where $V\in\{E,H\}$, $V_u=\tilde{G}_{zu}^V(\boldsymbol{\rho},\boldsymbol{\rho}')$, $k_\rho=\sqrt{k^2n^2-\beta^2}$, β is the propagation constant in the z coordinate, and

$$D_u^E=\delta_{zu}+\frac{i\beta}{k^2n(\mathbf{r})^2}\boldsymbol{\nabla}\cdot\tilde{\mathbf{u}} \text{ and } D_u^H=\tilde{\mathbf{z}}\cdot\boldsymbol{\nabla}\times\tilde{\mathbf{u}},$$

are simple differential operators. Equation (3) is solved using a multipole expansion, whereby the fields in the local coordinates of the lth cylinder are expressed in terms of cylindrical harmonics

$$V^l=\sum_{m=-\infty}^{\infty}[A_m^{Vl}J_m(k_\rho\rho_l)+B_m^{Vl}H_m^{(1)}(k_\rho\rho_l)]e^{im\phi_l}e^{i\beta z}. \tag{4}$$

Green's second theorem is used to derive the global field expansion

$$V_u=-\frac{i}{4}D_u^V\{H_0^{(1)}(k_\rho\rho_s)\}+\sum_{l=1}^{N_c}\sum_{m=-\infty}^{\infty}B_{um}^{Vl}H_m^{(1)}(k_\rho\rho_l)e^{im\,\phi_l}, \tag{5}$$

which applies throughout the background medium. Graf's addition theorem [23] is used to enforce the consistency of Eqs. (4) and (5) in the vicinity of the lth cylinder and yields the Rayleigh identity

$$A_{um}^{Vl}=K_{um}^V+\sum_{q=1,q\neq l}^{N_c}\sum_{p=-\infty}^{\infty}S_{mp}^{lq}B_{up}^{Vq}, \tag{6}$$

where

$$S_{mp}^{lq}=H_{m-p}^{(1)}(k_\rho\rho_q)e^{i(p-m)\phi_q},$$

and K_{um}^V is the source term composed of Bessel functions. The Rayleigh identity (6) reflects the observation that the local converging field A_m is due the diverging field from all other source bodies (B_m,K_m).

The field coefficients (A_m,B_m) are also linked by the boundary conditions at the cylinder surfaces [22], which when combined with Eq. (6) form a complete linear system. By employing a multipole formulation consistent with the geometry of the problem, the boundary conditions are enforced analytically rather than through a Fourier series. This has three significant benefits: (1) a simple semianalytic expression for the fields is obtained; (2) an elegant identity is obtained, from which the eigenvalue problem can be solved, and the field coefficients determined with a single-matrix inversion; and (3) convergence is superior to the alternative methods. Thus, the multipole method can be used to solve efficiently wave equations in an arbitrary arrangement of circular cylinders, but for structures that are finite in the (x,y) plane, is restricted to cylinders of infinite length.

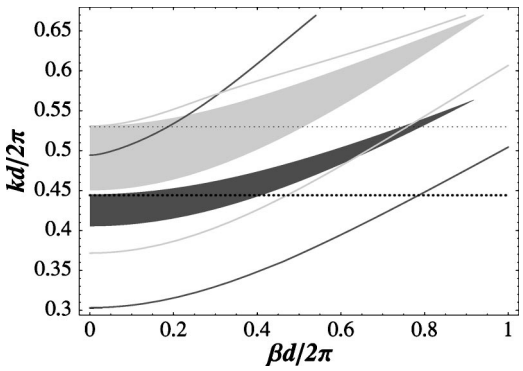

FIG. 1. Out-of-plane band structure showing the gap region emanating from the complete 2D band gap (shaded) and the bounds of the region from the TE band gap (solid lines). Parameters are $n_b=3.4$ with $a_l/d=0.45$ (dark gray) and $a_l/d=0.48$ (light gray). Dashed lines show where the complete gap region covers the widest range of propagation angles.

The dyadic Green's function is finally obtained by applying an inverse Fourier transformation, amounting to an integration over all β in the field expansions. The integral has poles on the real axis at $\beta=\pm k\,n$, and near the axis in the range $k\min(n_b,n_l)<|\beta|<k\max(n_b,n_l)$ corresponding to bound and leaky modes [22]. These are addressed using a contour integral in complex-β space. For $\mathrm{Re}\{\beta\}>0$, causality is enforced, after setting $\beta=Re^{i\theta}$, on a contour of the form

$$\mathbb{C}=\{\beta|0\leqslant R\leqslant R',\theta'\}\cup\{\beta|R',\theta'\leqslant\theta\leqslant 0\}$$
$$\cup\{\beta|R'\leqslant R<\infty,0\}, \tag{7}$$

with $\theta'\approx-\pi/4$ and $R'\approx 1.1k\max(n_b,n_l)$ found to optimize convergence. A similar contour above the axis is used for $\mathrm{Re}\{\beta\}<0$.

Macroporous silicon, with infrared refractive index $n_b=3.4$, is considered with cylinder radii of $a_l/d=0.45$ and $a_l/d=0.48$, where d is the lattice constant [19]. The important features of the relevant 3D out-of-plane band structure are shown in Fig. 1. For 2D in-plane propagation, the EM fields separate into a transverse electric (TE) and transverse magnetic (TM) mode. For both structures, the TM band gap lies inside the TE band gap forming a complete 2D band gap. For out-of-plane propagation, the modes exhibit a hybrid TE-TM nature due to the boundary conditions, and the complete 2D gap is projected into higher frequencies, indicated by the shaded regions in the figure. Though there is no complete 3D band gap, the gap region covers a broad range of propagation angles at the high frequency edge of the complete 2D band gap. The figure also shows the bounds of the gap region emanating from the TE band gap. Note that for a wider in-plane gap, the corresponding out-of-plane gap region covers a wider range of propagation angles.

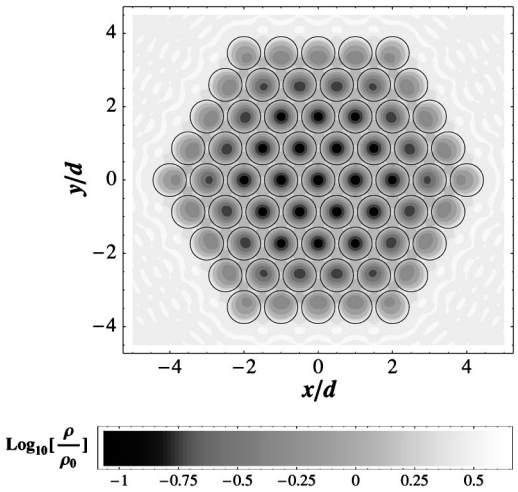

FIG. 2. The 3D LDOS taken across the plane of a hexagonal cluster of $N_c=61$ (4 rings) air voids in macroporous silicon with refractive index $n_b=3.4$. The cylinder radius is $a_l/d=0.45$ and the wave number is $kd/2\pi=0.442$. The LDOS is normalized to the free space value $\rho_0=k^2/\pi^2c$.

The 3D LDOS across the plane of a finite hexagonal sample of macroporous silicon ($kd/2\pi=0.442$, $a_l/d=0.45$) is shown in Fig. 2. The figure was produced with $4-6$ figure accuracy and a resolution of 400 points per unit cell using 12 h of computation time on one 2 GHz Pentium IV CPU. The spatial distribution of the LDOS is uniform inside the two outer hexagonal rings of cylinders, taking the same form in each unit cell. This is in contrast to the 2D LDOS in a finite 2D cluster of cylinders [16], which exhibits a variety of patterns in the spatial distribution, and rapid variations in these patterns near a band edge. The out-of-plane band structure draws in the projected 2D band structure over a range of frequencies, which dilutes these striking features. At the centers of the interior cylinders, the LDOS is suppressed by one order of magnitude from its value in free space. The LDOS then increases smoothly as the cylinder walls are approached, and is slightly enhanced in the background. In the two outer rings, the suppression is smaller, and is offset towards the center of the structure. Outside the structure, the LDOS rapidly attains the value $\rho=n_b\rho_0$ that it holds in a homogeneous medium with the refractive index of the background.

The dependence of the LDOS on cluster size is shown in Fig. 3. For a single cylinder, the difference inside and outside the cylinder simply reflects the refractive index contrast. As the number of rings increases, the Bragg effect becomes significant, causing stronger suppression inside the cylinders. Maximum suppression is limited to one order of magnitude, and suppression in the interior cylinders quickly saturates. This is in contrast to a complete gap structure, where suppression grows exponentially with cluster size [16]. Note that the LDOS is essentially the same in a ring with a given offset from the cluster edge, irrespective of cluster size, and ceases to change significantly inside the two outer rings. Thus, all features of the spatial distribution of the LDOS (Fig. 2) are reproduced in a cluster containing three or more rings, and only small clusters need be considered in either theoretical or experimental work.

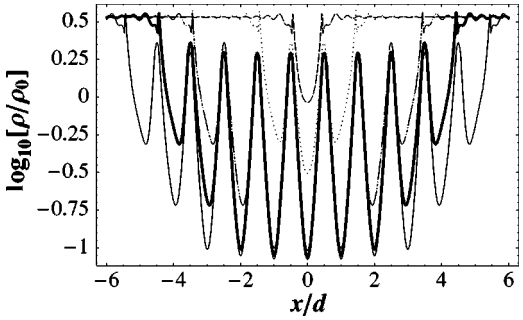

FIG. 3. The LDOS along the x axis for different sized clusters. The section of Fig. 2 ($N_c=61$) is shown (bold), along with $N_c=1$ (dashed), 7 (dotted), 37 (dash, dot, longdash, dotted), 91 (solid), otherwise using the same parameters.

The frequency dependence of the LDOS at the center of the structure for both $a_l/d=0.45$ and $a_l/d=0.48$ is shown in Fig. 4. Suppression with respect to vacuum is strongest at the top of the complete 2D band gap. The complete gap is widest at $a_l/d=0.48$, which produces maximum suppression of just under one order of magnitude [$\log_{10}(\rho/\rho_0)=-0.90$]. However, higher suppression of just over one order of magnitude [$\log_{10}(\rho/\rho_0)=-1.02$] can be achieved at $a_l/d=0.45$, for which the TE gap is much wider. The potential to obtain strong suppression in this class of PCs is limited by the absence of a complete 3D band gap. The width of the complete 2D band gap increases rapidly with the refractive index contrast [17], but the width of the TE gap is also clearly important, and it is not obvious that higher contrast would give much stronger suppression.

As a function of frequency, the LDOS is smooth and asymmetric about the top edge of the band gap, with a relatively sharp change on the high frequency side. This is a consequence of the upward sloping band structure and the top edge of the gap region having a flatter trajectory than the bottom edge. The change in the LDOS is sharpest for $a_l/d=0.45$, where its increase by $\Delta\log_{10}(\rho)=0.89$ occurs over a frequency range of $0.015(2\pi c/d)$, with a second smaller jump at the TE band edge. For $a_l/d=0.48$, where the top TE

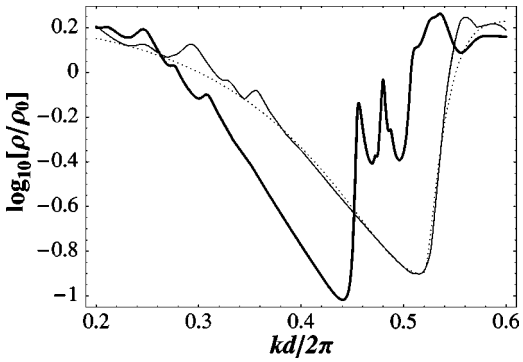

FIG. 4. The LDOS vs frequency at the center of the central cylinder for $N_c=37$, with $a_l/d=0.45$ (bold) and $a_l/d=0.48$ (thin). The analytic model (8) is shown with $\omega_c=0.52$, $h=0.93$, $\epsilon_\omega=4$ for $\omega<\omega_c$, $\epsilon_\omega=30$ for $\omega>\omega_c$ (dotted).

and TM band edges are contiguous, the jump is larger at over one order of magnitude [$\Delta \log_{10}(\rho) = 1.15$], but less abrupt, occurring over a frequency range of $0.044(2\pi c/d)$. For $d = 1.5\ \mu$m [19], the band edge wavelength is $\sim\lambda = 3.0\ \mu$m, and these jumps occur over wavelength ranges of $\Delta\lambda = 75$ nm and 160 nm, respectively.

The radiation dynamics in a pseudogap PC have previously been modeled analytically using a Gaussian function for the LDOS [24]. A similar asymmetric model can be applied to a 2D PC (Fig. 4), taking the form

$$\rho(\omega) = \rho_0(\omega)\{1 - h \exp[-(\epsilon_\omega(\omega - \omega_c))^2]\}, \qquad (8)$$

where ω_c is the band edge frequency, h describes the strength of the suppression, and ϵ_ω its width. To model the strong asymmetry in the LDOS, ϵ_ω is a step function with a much larger value for $\omega > \omega_c$ than for $\omega < \omega_c$. In this model, the LDOS is sufficiently smooth about the band edge for the usual Markovian assumption to apply.

In conclusion, an accurate and efficient method for calculating the LDOS in 2D PCs composed of cylinders has been demonstrated. The importance of the size of the structure and the spatial and frequency variation of the LDOS were investigated in macroporous silicon. Spontaneous emission can be suppressed by a significant one order of magnitude and rapidly saturates with cluster size, in contrast to the exponential decrease in the 2D LDOS. An asymmetric band edge model is appropriate for the 3D LDOS in a 2D PC, but the band edge jump is insufficient to lead to non-Markovian behavior. Because the multipole method applies to an arbitrary arrangement of cylinders, it can be used to examine the sensitivity of the LDOS to disorder, though this is outside the scope of this work. The EM Green's functions can also be used to obtain other important quantities such as the LDOS for a particular dipole orientation, or projected LDOS, and the Lamb shift.

The Australian Research Council supported this work.

[1] E. Yablonovitch, Phys. Rev. Lett. **58**, 2059 (1987).
[2] S. John, Phys. Rev. Lett. **58**, 2486 (1987).
[3] S. John and J. Wang, Phys. Rev. Lett. **64**, 2418 (1991).
[4] Y. Yang and S-Y. Zhu, Phys. Rev. A **62**, 013805 (2000).
[5] S. John and T. Quang, Phys. Rev. A **50**, 1764 (1994); S. John and T. Quang, Phys. Rev. Lett. **78**, 1888 (1997); M. Florescu and S. John, Phys. Rev. A **64**, 033801 (2001); S. John and T. Quang, Phys. Rev. Lett. **74**, 3419 (1995).
[6] Z-Y. Li, L-L. Lin, and Z-Q. Zhang, Phys. Rev. Lett. **84**, 4341 (2000).
[7] *Photonic Band Gap Materials*, edited by C.M. Soukoulis (Kluwer Academic, Dordrecht, 1996).
[8] J. Martorell and N.M. Lawandy, Phys. Rev. Lett. **65**, 1877 (1990); M. Megens *et al.*, J. Opt. Soc. Am. B **16**, 1403 (1999); T. Yamasaki and T. Tsutsui, Appl. Phys. Lett. **72**, 1957 (1998).
[9] E.P. Petrov *et al.*, Phys. Rev. Lett. **81**, 77 (1998); S.G. Romanov *et al.*, Appl. Phys. Lett. **75**, 1057 (1999); A.F. Koenderink *et al.*, Phys. Rev. Lett. **88**, 143903 (2002).
[10] R. Sprik, B.A. van Tiggelen, and A. Lagendijk, Europhys. Lett. **35**, 265 (1996).
[11] K. Busch and S. John, Phys. Rev. E **58**, 3896 (1998).
[12] V. Lousse *et al.*, Phys. Rev. B **64**, 201104 (2001).
[13] R.K. Lee, Y. Xu, and A. Yariv, J. Opt. Soc. Am. B **17**, 1438 (2000); C. Hermann and O. Hess, *ibid.* **19**, 3013 (2002).
[14] O.J.F. Martin *et al.*, Phys. Rev. Lett. **82**, 315 (1999).
[15] A. Moroz, Europhys. Lett. **46**, 419 (1999); M. Wubs and A. Lagendijk, Phys. Rev. E **65**, 046612 (2002).
[16] A.A. Asatryan *et al.*, Phys. Rev. E **63**, 046612 (2001); Opt. Express **8**, 191 (2001).
[17] R.D. Meade *et al.*, Appl. Phys. Lett. **61**, 495 (1992); J. D. Joannopoulos, R. D. Meade, and J. N. Winn, *Photonic Crystals: Molding the Flow of Light* (Princeton University Press, Princeton, 1995).
[18] M. Bayindir *et al.*, Phys. Rev. B **64**, 195113 (2001).
[19] U. Gruning, V. Lehmann, and C.M. Engelhardt, Appl. Phys. Lett. **68**, 747 (1996); J. Schilling *et al.*, J. Opt. A, Pure Appl. Opt. **3**, S121 (2001).
[20] B. Balian and C. Block, Ann. Phys. (Paris) **64**, 271 (1971).
[21] W.C. Chew, *Waves and Fields in Inhomogeneous Media* (IEEE Press, New York, 1995).
[22] T.P. White *et al.*, J. Opt. Soc. Am. B **19**, 2322 (2002).
[23] *Handbook of Mathematical Functions*, edited by M. Abramowitz and I.A. Stegun (Dover, New York, 1972).
[24] N. Vats, S. John, and K. Busch, Phys. Rev. A **65**, 043808 (2002).